Multistability in the Kuramoto model with synaptic plasticity

Yuri L. Maistrenko,[1,2] Borys Lysyansky,[1] Christian Hauptmann,[1] Oleksandr Burylko,[1,2] and Peter A. Tass[1,3]
[1]*Institute of Medicine and Virtual Institute of Neuromodulation, Research Centre Jülich, 52425 Jülich, Germany*
[2]*Institute of Mathematics, National Academy of Sciences of Ukraine, 01601 Kyiv, Ukraine*
[3]*Department of Stereotaxic and Functional Neurosurgery, University Hospital, 50924 Cologne, Germany*
(Received 10 November 2006; revised manuscript received 10 April 2007; published 18 June 2007)

We present a simplified phase model for neuronal dynamics with spike timing-dependent plasticity (STDP). For asymmetric, experimentally observed STDP we find multistability: a coexistence of a fully synchronized, a fully desynchronized, and a variety of cluster states in a wide enough range of the parameter space. We show that multistability can occur only for asymmetric STDP, and we study how the coexistence of synchronization and desynchronization and clustering depends on the distribution of the eigenfrequencies. We test the efficacy of the proposed method on the Kuramoto model which is, *de facto*, one of the sample models for a description of the phase dynamics in neuronal ensembles.

DOI: 10.1103/PhysRevE.75.066207 PACS number(s): 05.45.Xt, 87.18.Sn, 87.19.La

I. INTRODUCTION

Spike timing-dependent plasticity (STDP) is considered as being a fundamental mechanism for learning and memory in nervous systems [1,2]. A synapse conveys signals from a presynaptic to a postsynaptic neuron. Its strength crucially depends on the timing between the actions of the two neurons. It has been shown that if a presynaptic spike advances the postsynaptic spike, the synapse is potentiated (the synaptic weight increases), whereas in the opposite case the synapse is depressed (its weight decreases). The detailed molecular processes underlying STDP remain a matter of debate [1,2].

We here focus on the effects of STDP on macroscopic phenomena, especially on the STDP induced coexistence of distinct patterns of synchronization and connectivity in groups of oscillatory neurons. We choose a phenomenological level of description to reveal fundamental consequences of STDP action. For this, we incorporate STDP [1] into a generic network of phase oscillators, which approximates the dynamics of a network of synaptically interacting neurons (see [3–5]). A model neuron (i.e., phase oscillator) produces an action potential whenever its phase equals 0 mod 2π. We start with the Kuramoto model of coupled phase oscillators [3,7]

$$\dot{\theta}_i = \omega_i + \frac{1}{N}\sum_{j=1}^{N} K_{ij} g(\theta_i - \theta_j), \quad i = 1, \ldots, N, \tag{1}$$

where θ_i are the phases of the individual oscillators (i.e., neurons), ω_i are the natural frequencies (spiking rates), and K_{ij} are the coupling coefficients (synaptic weights). The coupling function reads $g(x) = -\sin x$. The Kuramoto model (1) has been used to study synchronization processes in various fields of the natural sciences (see, e.g., [3,6]) and in medicine [5].

A recent numerical study in the Kuramoto model with couplings subjected to STDP suggests that in a certain parameter range a desynchronized (weakly coupled) state coexists with a synchronized (strongly coupled) state [8]. We have investigated whether STDP generically leads to a coexistence of synchronized states and desynchronized states. In particular, we show that in the Kuramoto model STDP gives rise to a multistability of synchronized, desynchronized, and cluster states, provided the STDP learning rule is asymmetric, as observed in experiments.

II. MODEL

In the standard N-dimensional Kuramoto model without plasticity ($K_{ij} = K = \text{const}$), desynchronization occurs when the parameter K decreases below a critical bifurcation value K_c: The averaged frequencies $\bar{\omega}_i$ of the individual oscillators θ_i split from the common mean frequency $\Omega = \Sigma \omega_i / N$. The number of unequal frequencies $\bar{\omega}_i$ grows with further decreasing K until at some K_d full desynchronization is achieved. A generic property of the standard Kuramoto model without plasticity is an uniqueness of its limiting state (except for atypical narrow parameter regions at the borders between different states [7]).

In order to incorporate the mechanism of plasticity in the Kuramoto model (1), we assume that the elements of the coupling matrix K_{ij} are varied in accordance with the STDP learning rule: Let a presynaptic spike from the jth neuron arrive at the ith neuron at time t_{pre}, whereas a postsynaptic spike is generated in the ith neuron at time t_{post}. The value of K_{ij} increases (synaptic potentiation) or decreases (depression) depending on the sign of the spike-timing difference $\Delta t = t_{post} - t_{pre}$. A potentiation occurs when the postsynaptic spike follows the presynaptic spike, i.e., $\Delta t > 0$. Conversely, a depression takes place if $\Delta t < 0$. As shown experimentally [1], the amount of the change induced in the synaptic weight ΔK_{ij} decreases exponentially with increasing modulus of the spike-timing difference Δt as follows:

$$\Delta K_{ij} = \varepsilon_p (\alpha - K_{ij}) \exp\{-\Delta t/\tau_p\} \quad (\Delta t > 0),$$

$$\Delta K_{ij} = -\varepsilon_d K_{ij} \exp\{\Delta t/\tau_d\} \quad (\Delta t < 0).$$

The multiplier $\alpha - K_{ij}$ in the second relation is added to prevent from an unphysiological growth of the synaptic weights: this implies that all K_{ij} are positive and bounded by

the maximal coupling strength denoted by α. Moreover, potentiation is strong and depression is mild if the synapse is weak (i.e., if K_{ij} is small) and, conversely, potentiation is mild and depression strong if K_{ij} is large and close to α.

Going over to phase variables θ_i of Eq. (1) and taking into account the slow variation of K_{ij} with respect to the fast spiking dynamics, it is natural to rewrite the STDP rule in the time-continuous form

$$\dot{K}_{ij} = \varepsilon \begin{cases} (\alpha - K_{ij}) \exp\{(\theta_i - \theta_j)/\tau_p\}, & (\theta_i - \theta_j) \in [-\pi, 0] \\ -K_{ij} \exp\{-(\theta_i - \theta_j)/\tau_d\}, & (\theta_i - \theta_j) \in [0, \pi], \end{cases} \tag{2}$$

where, for simplicity, a unique small parameter ε (instead of two of them, ε_p and ε_d) is introduced.

The Kuramoto model with synaptic plasticity, Eqs. (1) and (2), is a system of N^2 ordinary differential equations defined on the Cartesian product of the N-dimensional torus $\mathbb{T}^N$ (phase variables θ_i) and the $N(N-1)$-dimensional Euclidean space $\mathbb{R}^{N(N-1)}$ (coupling variables K_{ij}). The STDP learning rule is asymmetric due to unequal coefficients τ_p and τ_d. In experiments [1], the coefficients are estimated as $\tau_p \simeq 16.8$ ms and $\tau_d \simeq 33.7$ ms, and hence, depression is approximately twice more effective than potentiation. In the numerical experiments below we mostly choose $\tau_p = 0.15$ and $\tau_d = 0.3$.

It is important that Eqs. (1) and (2), incorporate the main experimental and theoretical findings for the STDP learning rule (see [1,2], and references therein). Indeed, synaptic conductance equations (2) assume that strong synapses undergo relatively less potentiation than weak ones [due to the multiplier $(\alpha - K_{ij})$], whereas relative depression does not depend on the synaptic strength (given by the multiplier $-K_{ij}$). Competition between all synapses of a neuron in the network, and their automatic balance is established by the Kuramoto model (1). Actually, it controls the timing of postsynaptic spikes depending on all presynaptic spikes arriving to the neuron. Prevalence of depression compared to potentiation is determined by different exponents τ_d and τ_p, where $\tau_d > \tau_p$. Below we show that the asymmetry of the STDP learning rule is crucial for the multistability phenomenon. The phenomenon is manifested as coexistence of synchronized, desynchronized, and many other clustered states of different configurations in wide enough regions of the parameters space [12]. (In a Kuramoto model with a Hebbian, cosine synaptic learning rule coexistence of a special type of cluster states was found by [9]. The clusters there are a result of slow-fast motions in the degenerate case $\varepsilon \to 0$, where a synchronized group of oscillators joins desynchronized oscillators, which are uncoupled).

Before studying models (1) and (2), we note that—as will be shown below—the multistability phenomenon is neither significantly affected by varying the parameter ε (provided ε is not unphysiologically large enough; in that case multistability can disappear) nor by approximating the discontinuous functions in Eq. (2) by smooth ones (as proposed, e.g., by [10]). We demonstrate that the main dynamical features of the plasticity model are revealed already in the discontinuous case, which may be considered as the simplest STDP rule, which can further be elaborated.

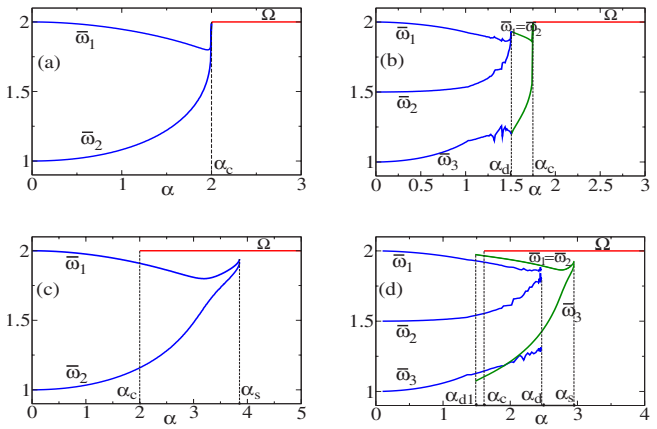

FIG. 1. (Color online) Frequency diagrams for Eqs. (1) and (2) with $N=2$ [(a),(c)] and $N=3$ [(b),(d)], and with an equally spaced distribution of the natural frequencies ω_i in the interval [1,2]. (a) and (b): no multistability for a symmetric STDP rule ($\tau_p = \tau_d = 0.3$); (c) and (d): multistability arises for an asymmetric STDP rule ($\tau_p = 0.15$, $\tau_d = 0.3$). Red: fully synchronized state with common frequency $\Omega = \omega_1$; blue: fully desynchronized states with different average frequencies $\bar{\omega}_i$; green: two-cluster states with $\bar{\omega}_1 = \bar{\omega}_2 \neq \bar{\omega}_3$. Parameter $\varepsilon = 0.5$.

III. STDP ASYMMETRY IMPLIES MULTISTABILITY

In this section we demonstrate that, when introducing plasticity in the Kuramoto model as proposed in Eqs. (1) and (2) the desynchronization transition changes its course from supercritical to subcritical, which happens only if the STDP rule is asymmetric [i.e., $\tau_d > \tau_p$ in Eqs. (2)]. Figure 1 illustrates a typical course of the desynchronization transition for $N=2$ and $N=3$ oscillators occurring for varying maximal coupling parameter α. For $\tau_d = \tau_p$ there is no mutistability: The desynchronization happens just at α_c when the fully synchronized state, given by a common frequency $\Omega = \omega_1$, disappears in a saddle-node bifurcation [Figs. 1(a) and 1(b)]. If the STDP rule is asymmetric, i.e., $\tau_d > \tau_p$, the situation is different: There exists an α-parameter interval, namely, for α between α_c and α_s, where the fully synchronized state coexists with a desynchronized state [$N=2$, Fig. 1(c)], or coexists with two desynchronized states [$N=3$, Fig. 1(d)] which are a fully desynchronized state of three different average frequencies $\bar{\omega}_1 \neq \bar{\omega}_2 \neq \bar{\omega}_3$ and a two-cluster state with average frequencies $\bar{\omega}_1 = \bar{\omega}_2 \neq \bar{\omega}_3$.

In general, we find that the multistability interval (α_c, α_s) arises in Eqs. (1) and (2) due to the asymmetry of the STDP rule, i.e., when τ_p becomes smaller than τ_d. There is an additional constraint for the existence of a nontrivial multistability interval: The parameter ε must not be large enough, e.g., in the case in Fig. 1(c) $\varepsilon < \varepsilon_M \approx 60.95$ has to be fulfilled). As illustrated in Fig. 4 below, the interval (α_c, α_s) expands with decreasing τ_p so that the length of (α_c, α_s) grows, probably, infinitely as τ_p tends to zero.

The mechanisms of the phenomenon can be visually illustrated in the simplest case of $N=2$ oscillators. Then, our

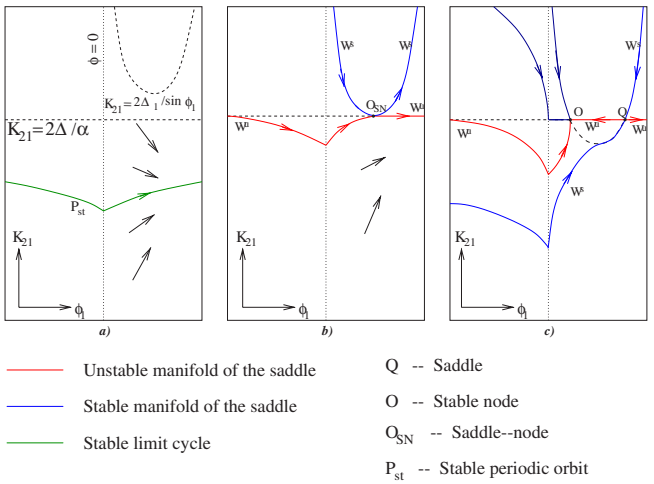

FIG. 2. (Color online) Schematic representation of the vector field transformations of the system (3) in the the symmetric case $\tau_p=\tau_d$, with increasing parameter α.

models (1) and (2) contains four equations; its state space is $\mathbb{T}^2\times\mathbb{R}^2$, but, the actual dynamics is three-dimensional: instead of two phases θ_1 and θ_2 one can introduce a phase difference variable $\varphi=\theta_1-\theta_2$ and then, the model is reduced to the form:

$$\dot{\varphi}=\Delta_1-\frac{K_{12}+K_{21}}{2}\sin\varphi,$$

$$\dot{K}_{12}=\varepsilon\begin{cases}(\alpha-K_{12})\exp\{\varphi/\tau_p\}, & \varphi\in[-\pi,0]\\ -K_{12}\exp\{-\varphi/\tau_d\}, & \varphi\in[0,\pi],\end{cases}$$

$$\dot{K}_{21}=\varepsilon\begin{cases}-K_{21}\exp\{\varphi/\tau_d\}, & \varphi\in[-\pi,0]\\ (\alpha-K_{21})\exp\{-\varphi/\tau_p\}, & \varphi\in[0,\pi],\end{cases}\qquad(3)$$

where $\Delta_1=\omega_1-\omega_2$. In the variables (φ,K_{12},K_{21}) the fully synchronized state is given by a stable fixed point $O=(\arcsin(2\Delta_1/\alpha),0,\alpha)$ of Eqs. (3), while the desynchronized regime is described by a stable periodic orbit P_{st} (see Figs. 2 and 3). The desynchronization transition happens at $\alpha_c=2\Delta_1$ and is caused by an annihilation of the stable node O and a saddle $Q=(\pi-\arcsin(2\Delta_1/\alpha),0,\alpha)$ in a saddle-node bifurcation at the point $O_{SN}=(\pi/2,0,\alpha)$. The course of the transition essentially depends on the equality (inequality) of the parameters τ_d and τ_p. In the symmetric case $\tau_d=\tau_p$, the saddle-node bifurcation at α_c is, at the same time, a homoclinic bifurcation for the saddle Q. The latter gives birth to a stable periodic orbit P_{st}. It exists for all $\alpha<\alpha_c$ and is just an image of the desynchronized state with different average frequencies $\bar{\omega}_1$ and $\bar{\omega}_2$ of the oscillators θ_1 and θ_2, respectively. See Fig. 2, where the transformations of the system vector field are shown, when α increases through α_c.

If $\tau_d>\tau_p$, the saddle-node bifurcation at α_c does not coincide with the homoclinic bifurcation and so, cannot give birth to a periodic orbit. We find that the stable periodic orbit P_{st} for the model (3) is born in this case in a different, greater coupling parameter value $\alpha_s>\alpha_c$ as a result of a cycle saddle-node bifurcation. In the bifurcation, P_{st} is born together with a saddle periodic orbit P_{sd}. Successive transformations of the vector field are presented in Fig. 3. It is shown that the homoclinic bifurcation of the saddle Q occurs at a parameter value α_h which lies in-between that of α_c and α_s, Fig. 3(c). The saddle periodic orbit P_{sd}, which is born there, moves in the direction to P_{st} with increasing α, and gets annihilated with P_{st} in the saddle-node bifurcation at α_s. The frequencies of the desynchronized states corresponding to P_{st} are visualized in Fig. 1(c).

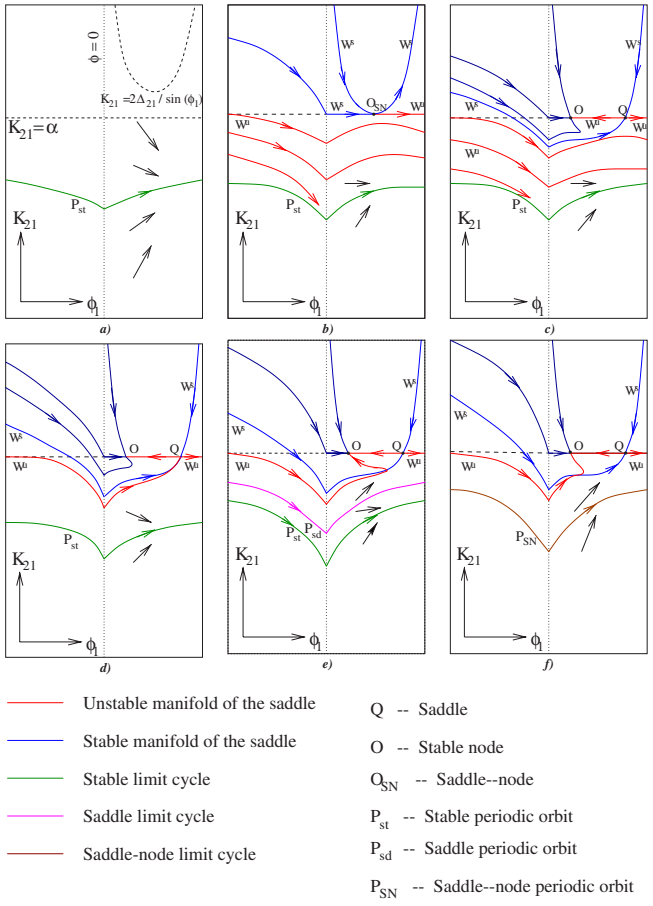

FIG. 3. (Color online) Schematic representation of the vector field transformations of the system (3) in the asymmetric case $\tau_p<\tau_d$, with increasing parameter α.

Figure 4 demonstrates how the size of the multistability interval (α_c,α_s) depends on the asymmetry of the STDP learning rule. In the figure, we fix $\tau_d=0.3$ and decrease τ_p from 0.3 (symmetric STDP rule) to zero. Then, the multistability interval (α_c,α_s) extends monotonically with decreasing τ_p and, as it is expected, its length grows infinitely as τ_p approaches zero. At the same time, the homoclinic bifurcation curve, denoted by H, is bounded and monotonically approaches a limiting value $\alpha_H^0\approx 2.25$ as $\tau_p\to 0$.

The synchronized state O with common frequency $\Omega=\omega_1$ is characterized by a unidirectional coupling scheme such that the faster oscillator (θ_1) drives the slower one (θ_2). Indeed, as can be easily concluded from the last two equations of Eqs. (3), in the synchronized, phase-locked regime $K_{12}=0$ and $K_{21}=\alpha$ hold. Also, as one can see, the phase shift between the synchronized oscillators is equal to $\pi/2$ at α_c

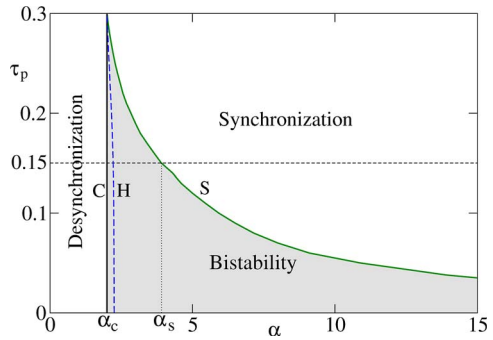

FIG. 4. (Color online) Different dynamical regimes on the parameter plane (α, τ_p). Parameters $\tau_d=0.3$, $\varepsilon=0.5$, $\omega_1=2$, and $\omega_1=1$.

and decreases to 0 with increasing $\alpha \to \infty$. The order parameter R of the synchronized state can be obtained in this case from the explicit formula

$$R = \left| \frac{1}{2} \sum_{j=i}^{2} e^{i\theta_j} \right| = \frac{1}{2} \sqrt{2\left(1 + \sqrt{1 - \frac{4\Delta_1^2}{\alpha^2}}\right)}.$$

Therefore, $R=\sqrt{2}/2$ at α_c and approaches 1 as $\alpha \to \infty$.

For the desynchronized state given by the cycle P_{st} both coupling coefficients K_{12} and K_{21} are nonzero and perform temporal oscillations between 0 and α. Moreover, the same holds for the sum of them: $0<K_{12}+K_{12}<\alpha$ provided that $\tau_d > \tau_p$. (In the symmetric case $\tau_d=\tau_p$ one gets $K_{12}+K_{12}=\alpha$). A typical dynamics of the coupling coefficients $K_{12}(t)$ and $K_{21}(t)$ is plotted in Fig. 5.

In the case of three globally coupled oscillators [$N=3$ in Eqs. (1) and (2)] the actual system dynamics is eight-dimensional and acting on $\mathbb{T}^2 \times \mathbb{R}^6$. The bifurcation structure in that case is much more complicated, nevertheless, as illustrated in Figs. 1(b) and 1(d), the course of the desynchronization transition is generally similar to the $N=2$ case. In particular, the fully synchronized phase-locked state O is given by the maximal frequency $\Omega=\omega_1$. It disappears with decreasing α in a saddle-node bifurcation at a critical bifurcation value α_c. [The value of α_c is different from the $N=2$ case (see the next chapter)]. Two nonsynchronized states, a desynchronized and a clustered, end in cycle saddle-node

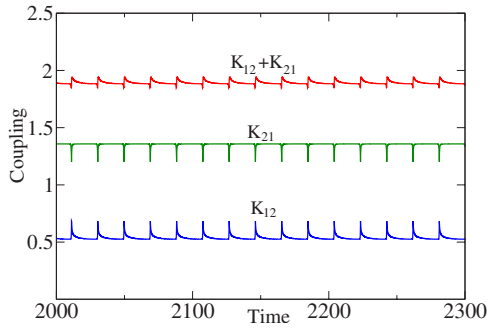

FIG. 5. (Color online) Typical graphs of the variables $K_{12}(t)$ and $K_{21}(t)$, and their sum $K_{12}(t)+K_{21}(t)$. Parameters $\alpha=3.0$, $\tau_p=0.15$, $\tau_d=0.3$, $\varepsilon=0.5$, $\omega_1=2$, and $\omega_1=1$.

bifurcations at α_d and α_s, respectively. By the analogy with the $N=2$ case, we suggest that saddle periodic orbits which are born in the saddle-node bifurcations last with decreasing α up to respective homoclinic bifurcations, where they cease to exist. We leave "further detailizing" of the $N=3$ bifurcation structure for future study.

IV. SYNCHRONIZED PHASE-LOCKED STATE

In this section we perform a complete analytical analysis of the fully synchronized state of Eqs. (1) and (2), denoted as O. O is given by a unique stable equilibrium of the reduced system in phase differences $\varphi_i=\theta_1-\theta_{i+1}$ as follows:

$$\dot{\varphi}_i = \Delta_i - \frac{1}{N}\left[(K_{1,i+1} + K_{i+1,1})\sin\varphi_i + \sum_{j=1, j\neq i}^{N-1} [K_{1,j+1}\sin\varphi_j + K_{i+1,j+1}\sin(\varphi_i - \varphi_j)] \right], \quad (4)$$

where $\Delta_i=\omega_1-\omega_{i+1}$, $i=1,\ldots,N-1$. To find O, note that in any equilibrium point of Eqs. (4) and (2), each K_{ij} equals either 0 or α [which follows from Eq. (2) due to phase locking of O]. Suppose for definiteness, all natural frequencies ω_i be different and ordered as $\omega_1>\omega_2>\cdots>\omega_N$. This implies $K_{ij}=\alpha$ for $i>j$, and $K_{ij}=0$ else. By substituting the values of K_{ij} into Eq. (4), one can get O from the skew-product system

$$\Delta_i - \frac{\alpha}{N}\left[\sin\varphi_i + \sum_{l=1}^{i-1} \sin(\varphi_i - \varphi_l) \right] = 0, \quad i = \overline{1, N-1}. \quad (5)$$

This implies, in particular, that the common frequency Ω of the synchronized state O is equal to the maximal natural frequency ω_1. Indeed, in the synchronized phase-locked state all $K_{1j}=0$, so that the first equation of Eq. (1) is reduced to $\dot{\theta}_1=\omega_1$. The other phases θ_i rotate with the same frequency ω_1 due to the phase locking. It follows from Eq. (5) that the existence and stability of the state O is defined by relations between the differences of the natural frequencies $\Delta_i=\omega_1-\omega_{i+1}$ and the parameter α, and is not affected by the other parameters ε, τ_1, and τ_2 (nevertheless, the latter control the basin of O). It is important to point out that in the synchronized phase-locked state O, the coupling between the oscillators is unidirectional and downwards oriented, i.e., from oscillators with greater to smaller eigenfrequencies.

Summing up the results of this section we formulate the following:

Theorem. There exists a critical coupling parameter value $\alpha_c>0$, which depends on the distribution of the natural frequencies $\omega_1, \omega_2, \ldots, \omega_N$, but does not depend on the other parameters τ_1, τ_2, and $\varepsilon>0$, such that

(1) for $\alpha \geqslant \alpha_c$, the Kuramoto model with synaptic plasticity, Eqs. (1) and (2), has the synchronized phase-locking state O given by the unique stable equilibrium of Eqs. (5). The synchronized state is characterized by an hierarchical unidirectional coupling structure, where the fastest oscillator imposes its frequency on all others;

(2) there is no synchronized phase-locked states for $\alpha < \alpha_c$.

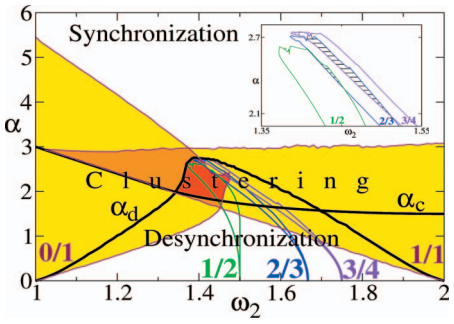

FIG. 6. (Color) Two-parameter multistability diagram for Eqs. (1) and (2) with $N=3$. Horizontal axis: ω_2 varies between $\omega_3=1$ and $\omega_1=2$; vertical axis: α. Regions of synchronization (for $\alpha \geqslant \alpha_c$) and full desynchronization (for $\alpha < \alpha_d$) are delineated by bold curves α_c and α_d. Two clustering regions given by the resonant tongues $C_{0/1}$ and $C_{1/1}$ are shown in yellow. They overlap in orange and red regions where three and four different states, respectively, coexist. Overlap of the main resonant tongues $D_{1/2}$, $D_{2/3}$, and $D_{3/4}$ is illustrated in the inset. Parameters $\tau_p=0.15$, $\tau_d=0.3$, $\varepsilon=0.5$.

From Eq. (5) we obtain in the simplest $N=2$ case $\alpha_c = 2\Delta_1$ (see Sec. III for details). We have also explicitly found α_c for the case of $N=3$ oscillators as follows:

$$\alpha_c = \min\left\{3\Delta_1;\ \frac{3\Delta_2^2}{2\sqrt{\Delta_2^2-\Delta_1^2}}\right\}$$

(valid under the condition $\Delta_2 > \Delta_1 > 0$).

V. MULTISTABILITY VERSUS NATURAL FREQUENCIES

The simplest nontrivial case, when different desynchronized states coexist is given by three coupled oscillators [$N=3$ in Eqs. (1) and (2)]. In Fig. 6 a two-parameter bifurcation diagram is plotted which shows the multistability dynamics under a variation of the natural frequencies. For this, ω_1 and ω_3 are fixed, and ω_2 is varied. Four different dynamical regimes emerge depending on the parameters ω_2 and α: the fully synchronized state O (above the bifurcation curve α_c); the fully desynchronized state D (below the curve α_d); and two 2-cluster states $C_{0/1}$ and $C_{1/1}$ with average frequencies $\bar{\omega}_1=\bar{\omega}_2\neq\bar{\omega}_3$ and $\bar{\omega}_1\neq\bar{\omega}_2=\bar{\omega}_3$, respectively (in the yellow region; their overlap is shown in orange and red). As one can see, for any fixed ω_2 there exists at least one α-parameter interval where the synchronous state coexists with the cluster states and with the fully desynchronized state. The "most multistable" parameter region, where all four states coexist is shown in red. In Fig. 7, a one-dimensional frequency diagram for $\omega_2=1.4$ is presented, which appears to be much more complicated compared to the diagram with $\omega_2=1.5$ [Fig. 1(d)]. O, $C_{0/1}$, $C_{1/1}$, and D coexist in the parameter interval $1.9\ldots\leqslant\alpha\leqslant 2.7\ldots$ and, in addition, two coexisting fully desynchronized states can be recognized in a narrow parameter interval around $\alpha\approx 2.4$ (indicated by an arrow).

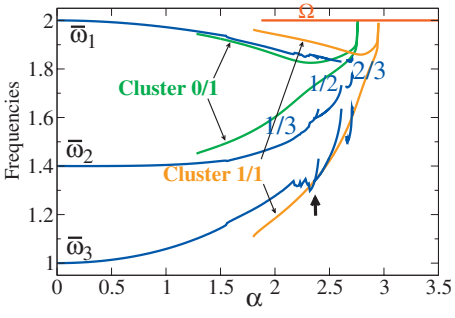

FIG. 7. (Color) Frequency diagram for Eqs. (1) and (2) with $N=3$. $\omega_2=1.4$; the other parameters as in Fig. 6. The arrow indicates coexistence of two different fully desynchronized states.

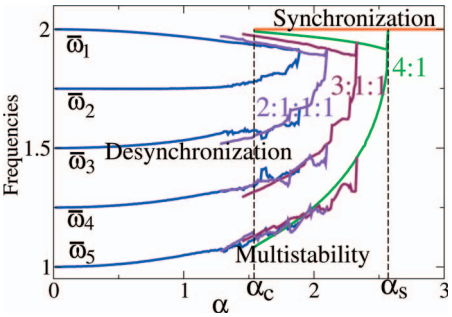

FIG. 8. (Color) Frequency diagram for Eqs. (1) and (2) with $N=5$; $\omega_i=2-(i-1)/(N-1)$, $i=1,\ldots,N$. Other parameters as before.

The multistability phenomenon in the models (1) and (2) can be interpreted as an intersection of resonant tongues $D_{p/q}$ originating from rational points at $\alpha=0$, where the dynamics of Eqs. (1) and (2) inside $D_{p/q}$ are characterized by the rotation number $p/q=(\bar{\omega}_2-\bar{\omega}_3)/(\bar{\omega}_1-\bar{\omega}_3)$. Three main resonant tongues $D_{1/2}$, $D_{2/3}$, and $D_{3/4}$ are shown in Fig. 6. Their intersection is illustrated in the inset. Moreover, the stability regions for the two-cluster states $C_{0/1}(\bar{\omega}_1=\bar{\omega}_2\neq\bar{\omega}_3)$ and

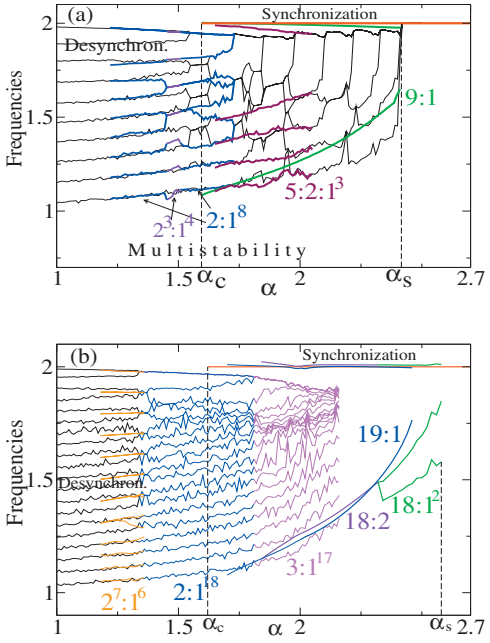

FIG. 9. (Color) Frequency diagram for Eqs. (1) and (2) with (a) $N=10$, (b) $N=20$; $\omega_i=2-(i-1)/(N-1)$, $i=1,\ldots,N$.

$C_{1/1}(\bar{\omega}_2=\bar{\omega}_3\neq\bar{\omega}_1)$ can also be considered as tongues $D_{0/1}$ and $D_{1/1}$, respectively.

VI. MANY COUPLED OSCILLATORS

The phenomenon of multistability becomes more developed with an increase of the network size N. Figure 8 illustrates a multistable transition from full synchronization to full desynchronization in Eqs. (1) and (2) for $N=5$ oscillators. The desynchronization transition starts at α_s, where the slowest oscillator θ_5 splits from the others, which remain synchronized: a two-cluster state emerges (shown in green) which coexists with the fully synchronized state (red). With further decreasing α, the second slowest oscillator θ_4 splits, which, in turn, results in a three-cluster state and so on. Therefore, for the $N=5$ case (see Fig. 8), four "standard" desynchronized states occur successively: 4:1; 3:1:1; 2:1:1:1; and 1:1:1:1:1 (integers denote the number of synchronized oscillators ϕ_i within a cluster with increasing index i).

In the network of $N=10$ oscillators, Fig. 9(a), the fully desynchronized state (thin black) ranges from $\alpha=0$ to $\alpha=1.52\ldots$, where it transforms into a six-cluster state $2^4:1^2$. With further increasing α, as one can see by a more detailed examination of Fig. 8(b), many other cluster states emerge successively, e.g., $2:1^8$, $3^2:2:1^2$, $3:1^7$, $3:2^3:1$, $4^2:1^2$, $5:2:1^3$, $6:2:1^2$, $7:1^3$, $8:1^2$, and 9:1. In the end, the fully synchronized state shows up as a global attractor for $\alpha>\alpha_s$. When calculating the bifurcation diagram with decreasing α, one can verify that these states exist and are stable at substantially longer parameter intervals compared to the forward calculations. In Fig. 9(a), graphs of the average frequencies for the states 9:1 (green), $5:2:1^3$ (maroon), and $2:1^8$ (blue) at their stability intervals are presented. Stability intervals for the other states are also long enough and typically include the critical bifurcation point α_c (we do not plot more states for the sake of clarity).

In Fig. 9(b), the multistability phenomenon is illustrated for $N=20$ oscillators. One can observe different cluster states and moreover, the multistability interval (α_c,α_s), where the cluster states coexist with full synchronization, appears to be even longer than in the $N=10$ case. In the figure, two groups of clusters can be clearly distinguished: (i) close to synchronization: 20 (full synchronization), 19:1, $18:1^2$, 18:2, and (ii) close to desynchronization: 1^{20} (full desynchronization), $2^7:1^6$, $2:1^{18}$, $3:1^{17}$.

Further increasing the number N of the oscillators in the network meets computational difficulties because of fast growing the dimension of Eqs. (1) and (2), which is equal to N^2. We have made longlasting calculations up to $N=50$ oscillators [then systems (1) and (2) contain 2500 equations] with randomly chosen initial conditions to detect coexistence of different states, and to clarify if the averaged order parameter

$$R=\lim_{T\to\infty}\frac{1}{T}\int_0^T\left|\frac{1}{N}\sum_{j=1}^{N}\exp(i\theta_j(t))\right|dt \qquad (6)$$

for the desynchronized states (fully desynchronized or clustered) decreases in accordance with the scale law $1/\sqrt{N}$ as N increases. As we have found, if the coupling parameter α lies in the desynchronized parameter interval (i.e., approximately α does not exceed the value 1.25) then indeed, R scales in this way. In Fig. 10 perfect agreement with the law is demonstrated for the parameter value $\alpha=1.0$ (black circles). In contrast, in the multistability parameter interval, which is the main subject of our study, there is no such "good" scaling behavior of R. Rather (e.g., for $\alpha=1.9$), with an increase of N up to 50, R saturates at around 0.41 ± 0.02 (green squares). The desynchronized solutions are normally not fully desynchronized in this case.

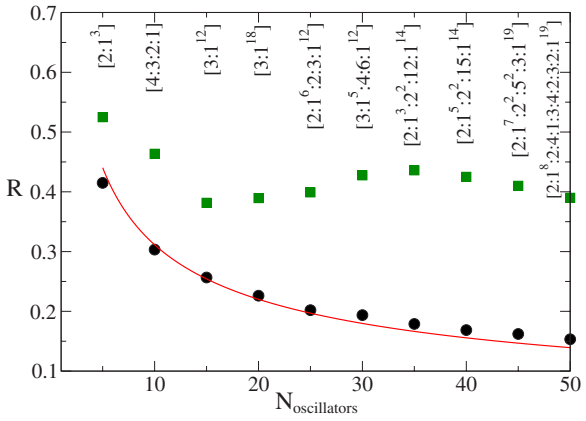

FIG. 10. (Color online) Averaged order parameter R of the desynchronized solutions versus the number of oscillators N. Black circles: fully desynchronized solutions for $\alpha=1.0$ and a direct fit $R=C/\sqrt{N}$ by the method of least squares (red); green squares: cluster solutions for $\alpha=1.9$ of the configurations shown above.

The nondecreasing behavior of the order parameter R in the multistability interval can be explained by the fact that the desynchronized solutions there are not fully desynchronized but clustered only. Indeed, some part of the oscillators in the solutions creates clusters of equal frequencies, other oscillators split off and rotate with different speeds. The number of the oscillators in the clusters can essentially change when varying N and moreover, as one can see in Figs. 7–9, many different cluster states can coexist in the multistability interval. For example, for $N=50$ we found coexistence of the fully synchronized state, when all frequencies are the same and equal to 2.0 ($R\approx0.80$) with two cluster states of the form: $2:1^8:2:4:1:3:4:2:3:2:1^{19}$ ($R\approx0.39$) and $2:1^{20}:2^3:1:2:1^{19}$ ($R\approx0.48$). It would be of big interest to clarify what is happening to the order parameter for larger $N>50$, which could be a subject of a future study with a focus on much more time consuming numerics.

To estimate the basin of attraction of different cluster states, we performed calculations of Eqs. (1) and (2) for fixed $\alpha=2.0$ and with randomly chosen initial conditions. The results, which are presented in Fig. 11 in the $N=5$ and $N=20$ cases, show that the size of the basins of attraction of both synchronized and desynchronized regimes, are large enough so that both types of states actually coexist, and therefore, each of these states can be reliably reached by established stimulation protocols [5,8].

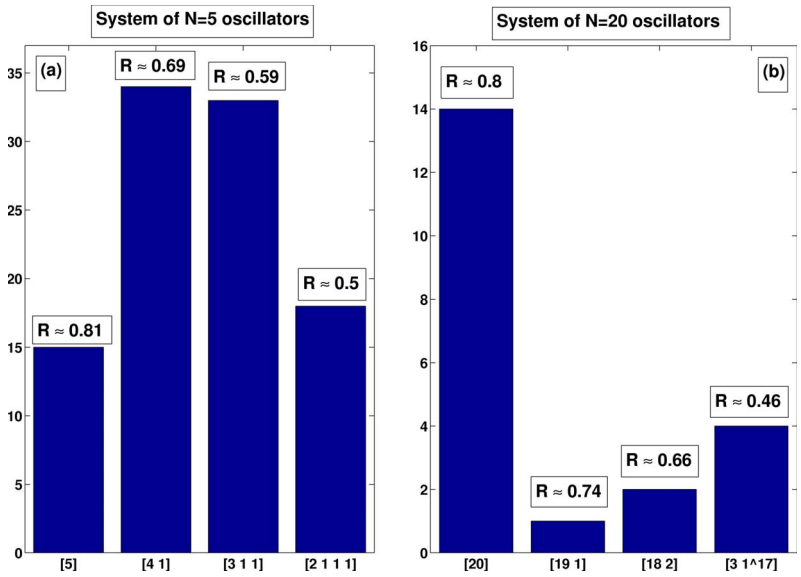

FIG. 11. (Color online) Histograms showing the frequency of different stable states of the model for (a) $N=5$ and (b) $N=20$, where Eqs. (1) and (2) were integrated with randomly chosen initial conditions. Averaged values of the order parameter R for the cluster states are also shown.

VII. CONCLUSION

In low-dimensional networks of phase oscillators with STDP we have revealed the mechanism leading to multistability. In addition to the results presented here, we found that the multistability becomes more developed by increasing the asymmetry of the STDP rule. Due to STDP, a plethora of coexisting stable cluster states emerges along with the completely synchronized and completely desynchronized states. Intriguingly, a statistical estimation of the basin boundaries of the multitude of attractors reveals that strongly synchronized and strongly desynchronized states are the dominating attractors (Fig. 11). This corresponds to numerical findings in the Kuramoto model with STDP [8] as well as in microscopic neural networks with symmetric STDP [11], both with a large number of oscillators or neurons.

We hypothesize that this low-dimensional mechanism controls also the multistability in the general N-dimensional Kuramoto model with STDP, and that the number of cluster states of different configuration, coexisting with full synchronization, grows at least proportionally to N. Our results suggest, that long-lasting changes of the network's connectivity can be induced with transient desynchronizing stimuli which shift the system from a stable synchronized state to a stable desynchronized or weakly synchronized state, where the system remains without further intervention. By the same token, periodic stimulations may shift the network from a stable desynchronized state to a stable synchronized state. Theoretical studies indicate that stimulation induced reshaping of neural networks may be relevant for the development of novel brain stimulation techniques (see [8,11]). In this way it would no longer be necessary to continuously suppress pathological synchronization. Rather, by exploiting STDP, one could achieve long-lasting effects by therapeutically rewiring the target network (see [8,11]). Of course, the affected brain areas are more complex than a population of phase oscillators. Rather, these brain areas consist of different types of neurons, some being excitatory, others inhibitory. Only a certain percentage of the whole mixed population of neurons appears to be involved in the pathological synchronization processes. Accordingly, our results may serve as a first step performed in a simple model, which can then be extended to a more complex models, containing, e.g., different types of microscopic model neurons.

ACKNOWLEDGMENTS

We are grateful to L. Tsimring, W. Gerstner, and M. Bazhenov for stimulating discussions. This study was supported by the Network of Excellence in Biosimulation (Grant No. 005137) and by IBM.

[1] H. Markram, J. Lübke, M. Frotscher, and B. Sakmann, Science **275**, 213 (1997); G. Q. Bi and M. Poo, J. Neurosci. **18**, 10464 (1998); Annu. Rev. Neurosci. **24**, 139 (2001); G. M. Wittenberg and S. S.-H. Wang, J. Neurosci. **26**, 6610 (2006); J.-P. Pfister and W. Gerstner, *ibid.* **26**, 9673 (2006).

[2] S. Song, K. D. Miller, andL. F. Abbott, Nat. Neurosci. **3**, 919 (2000); M. van Rossum and G. Turrigiano, Neurocomputing **38-40**, 409 (2001).

[3] Y. Kuramoto, *Chemical Oscillations, Waves and Turbulence* (Springer-Verlag, Berlin, 1984); S. H. Strogatz, Physica D **143**, 1 (2000).

[4] D. Hansel, G. Mato, and C. Meunier, Europhys. Lett. **23**, 367 (1993).

[5] P. A. Tass, *Phase Resetting in Medicine and Biology* (Springer, Berlin, 1999); Europhys. Lett. **55**, 171 (2001); **59**, 199 (2002); Phys. Rev. E **66**, 036226 (2002); **67**, 051902 (2003); Biol. Cybern. **89**, 81 (2003).

[6] G. Kozyreff, A. G. Vladimirov, and P. Mandel, Phys. Rev.

Lett. **85**, 3809 (2000); Y. B. Kazanovich and R. M. Borisyuk, Neural Networks **12**, 149 (1999); L. S. Tsimring N. F. Rulkov, M. L. Larsen, and M. Gabbay, Phys. Rev. Lett. **95**, 014101 (2005); H. Kori and Y. Kuramoto, Phys. Rev. E **63**, 046214 (2001); D. Pazó, *ibid.* **72**, 046211 (2005).

[7] Y. Maistrenko, O. Popovych, O. Burylko, and P. A. Tass, Phys. Rev. Lett. **93**, 084102 (2004); O. V. Popovych, Yu. L. Maistrenko, and P. A. Tass, Phys. Rev. E **71**, 065201(R) (2005).

[8] P. A. Tass and M. Majtanik, Biol. Cybern. **94**, 58 (2006).

[9] P. Seliger, S. C. Young, and L. S. Tsimring, Phys. Rev. E **65**, 041906 (2002).

[10] H. D. I. Abarbanel, R. Huerta, and M. I. Rabinovich, Proc. Natl. Acad. Sci. U.S.A. **99**, 10132 (2002).

[11] P. A. Tass and C. Hauptmann, **9**, 298 (2006); C. Hauptmann and P. A. Tass, BioSystems **89**, 173 (2007); P. A. Tass and C. Hauptmann, Int. J. Psychophysiol **64**, 53 (2007).

[12] By synchronized (clustered) state we mean a state where all oscillators (at least one group of oscillators) are characterized by the same average frequency, i.e., are phase locked. In the model considered, Eqs. (1) and (2), the synchronized oscillators are normally phase shifted with respect to each other, or they can oscillate with respect to each other with bounded phase difference. Fully desynchronized state means a state with all average frequencies being different.